Vacuum stability by vector dark matter

Bohdan GRZADKOWSKI
University of Warsaw

- The Vector Dark Matter (VDM) model
- Vacuum stability
- Landau poles
- Experimental constraints
- Direct detection of dark matter
- Summary

◇ Mateusz Duch, B.G., Moritz McGarrie, "A stable Higgs portal with vector dark matter", e-Print: arXiv:1506.08805

The Vector Dark Matter (VDM) model

- T. Hambye, "Hidden vector dark matter", JHEP 0901 (2009) 028,
- O. Lebedev, H. M. Lee, and Y. Mambrini, "Vector Higgs-portal dark matter and the invisible Higgs", Phys.Lett. B707 (2012) 570,
- Y. Farzan and A. R. Akbarieh, "VDM: A model for Vector Dark Matter", JCAP 1210 (2012) 026,
- S. Baek, P. Ko, W.-I. Park, and E. Senaha, "Higgs Portal Vector Dark Matter : Revisited", JHEP 1305 (2013) 036,
- Ch. Gross, O. Lebedev, Y. Mambrini, "Non-Abelian gauge fields as dark matter", arXiv:1505.07480,
- $\cdots$

The model:

- extra $U(1)_X$ gauge symmetry (A_X^μ),
- a complex scalar field S, whose vev generates a mass for the $U(1)$'s vector field, $S = (0, \mathbf{1}, \mathbf{1}, 1)$ under $U(1)_Y \times SU(2)_L \times SU(3)_c \times U(1)_X$.
- SM fields neutral under $U(1)_X$,
- in order to ensure stability of the new vector boson a $\mathbb{Z}_2$ symmetry is assumed to forbid $U(1)$-kinetic mixing between $U(1)_X$ and $U(1)_Y$. The extra gauge boson A_μ and the scalar S field transform under $\mathbb{Z}_2$ as follows

$$A_X^\mu \to -A_X^\mu \ , \ S \to S^*, \text{ where } S = \phi e^{i\sigma}, \ \ \mathrm{so} \ \ \phi \to \phi, \ \ \sigma \to -\sigma.$$

The scalar potential

$$V = -\mu_H^2|H|^2 + \lambda_H|H|^4 - \mu_S^2|S|^2 + \lambda_S|S|^4 + \kappa|S|^2|H|^2.$$

The vector bosons masses:

$$M_W = \frac{1}{2}gv, \qquad M_Z = \frac{1}{2}\sqrt{g^2 + g'^2}v \quad \text{and} \quad M_{Z'} = g_x v_x,$$

where

$$\langle H \rangle = \begin{pmatrix} 0 \\ \frac{v}{\sqrt{2}} \end{pmatrix} \text{ and } \langle S \rangle = \frac{v_x}{\sqrt{2}}$$

Positivity of the potential implies

$$\lambda_H > 0, \quad \lambda_S > 0, \quad \kappa > -2\sqrt{\lambda_H \lambda_S}.$$

The minimization conditions for scalar fields

$$(2\lambda_H v^2 + \kappa v_x^2 - 2\mu_H^2)v = 0 \text{ and } (\kappa v^2 + 2\lambda_S v_x^2 - 2\mu_S^2)v_x = 0$$

For $\kappa^2 < 4\lambda_H\lambda_S$ the global minima are

$$v^2 = \frac{4\lambda_S\mu_H^2 - 2\kappa\mu_S^2}{4\lambda_H\lambda_S - \kappa^2} \quad \text{and} \quad v_x^2 = \frac{4\lambda_H\mu_S^2 - 2\kappa\mu_H^2}{4\lambda_H\lambda_S - \kappa^2}$$

Both scalar fields can be expanded around corresponding vev's as follows

$$S = \frac{1}{\sqrt{2}}(v_x + \phi_S + i\sigma_S) \quad , \quad H^0 = \frac{1}{\sqrt{2}}(v + \phi_H + i\sigma_H) \quad \text{where} \quad H = \begin{pmatrix} H^+ \\ H^0 \end{pmatrix}.$$

The mass squared matrix $\mathcal{M}^2$ for the fluctuations (ϕ_H, ϕ_S) and their eigenvalues read

$$\begin{aligned} \mathcal{M}^2 &= \begin{pmatrix} 2\lambda_H v^2 & \kappa v v_x \\ \kappa v v_x & 2\lambda_S v_x^2 \end{pmatrix} \\ M_\pm^2 &= \lambda_H v^2 + \lambda_S v_x^2 \pm \sqrt{\lambda_S^2 v_x^4 - 2\lambda_H\lambda_S v^2 v_x^2 + \lambda_H^2 v^4 + \kappa^2 v^2 v_x^4} \end{aligned}$$

$$\mathcal{M}^2_{\text{diag}} = \begin{pmatrix} M_{h_1}^2 & 0 \\ 0 & M_{h_2}^2 \end{pmatrix}, \quad R = \begin{pmatrix} \cos\alpha & -\sin\alpha \\ \sin\alpha & \cos\alpha \end{pmatrix}, \quad \begin{pmatrix} h_1 \\ h_2 \end{pmatrix} = R^{-1} \begin{pmatrix} \phi_H \\ \phi_S \end{pmatrix},$$

where $M_{h_1} = 125.7$ GeV is the mass of the observed Higgs particle. Then we obtain

$$\sin 2\alpha = \frac{\text{sign}(\lambda_{SM} - \lambda_H)\, 2\mathcal{M}_{12}^2}{\sqrt{(\mathcal{M}_{11}^2 - \mathcal{M}_{22}^2)^2 + 4(\mathcal{M}_{12}^2)^2}}, \quad \cos 2\alpha = \frac{\text{sign}(\lambda_{SM} - \lambda_H)(\mathcal{M}_{11}^2 - \mathcal{M}_{22}^2)}{\sqrt{(\mathcal{M}_{11}^2 - \mathcal{M}_{22}^2)^2 + 4(\mathcal{M}_{12}^2)^2}}.$$

Note that since vev of H is fixed at 246.22 GeV, with $\kappa = 0$ (no mass mixing) and $\lambda_H \neq \lambda_{SM}$ it is only ϕ_S which can have the observed Higgs mass of 125.7 GeV. Even though the mass matrix is diagonal in this case, however in order to satisfy our convention that $M_{h_1} = 125.7$ GeV a rotation by $\alpha = \pm\pi/2$ is required in such a case.

There are 5 real parameters in the potential: μ_H, μ_S, λ_H, λ_S and κ. Adopting the minimization conditions μ_H, μ_S could be replaced by v and v_x. The SM vev is fixed at $v = 246.22$ GeV. Using the condition $M_{h_1} = 125.7$ GeV, v_x^2 could be eliminated in terms of $v^2, \lambda_H, \kappa, \lambda_S, \lambda_{SM} = M_{h_1}^2/(2v^2)$:

$$v_x^2 = v^2 \frac{4\lambda_{SM}(\lambda_H - \lambda_{SM})}{4\lambda_S(\lambda_H - \lambda_{SM}) - \kappa^2}$$

Eventually there are 4 independent parameters:

$$(\lambda_H, \kappa, \lambda_S, g_x),$$

where g_x is the $U(1)_X$ coupling constant.

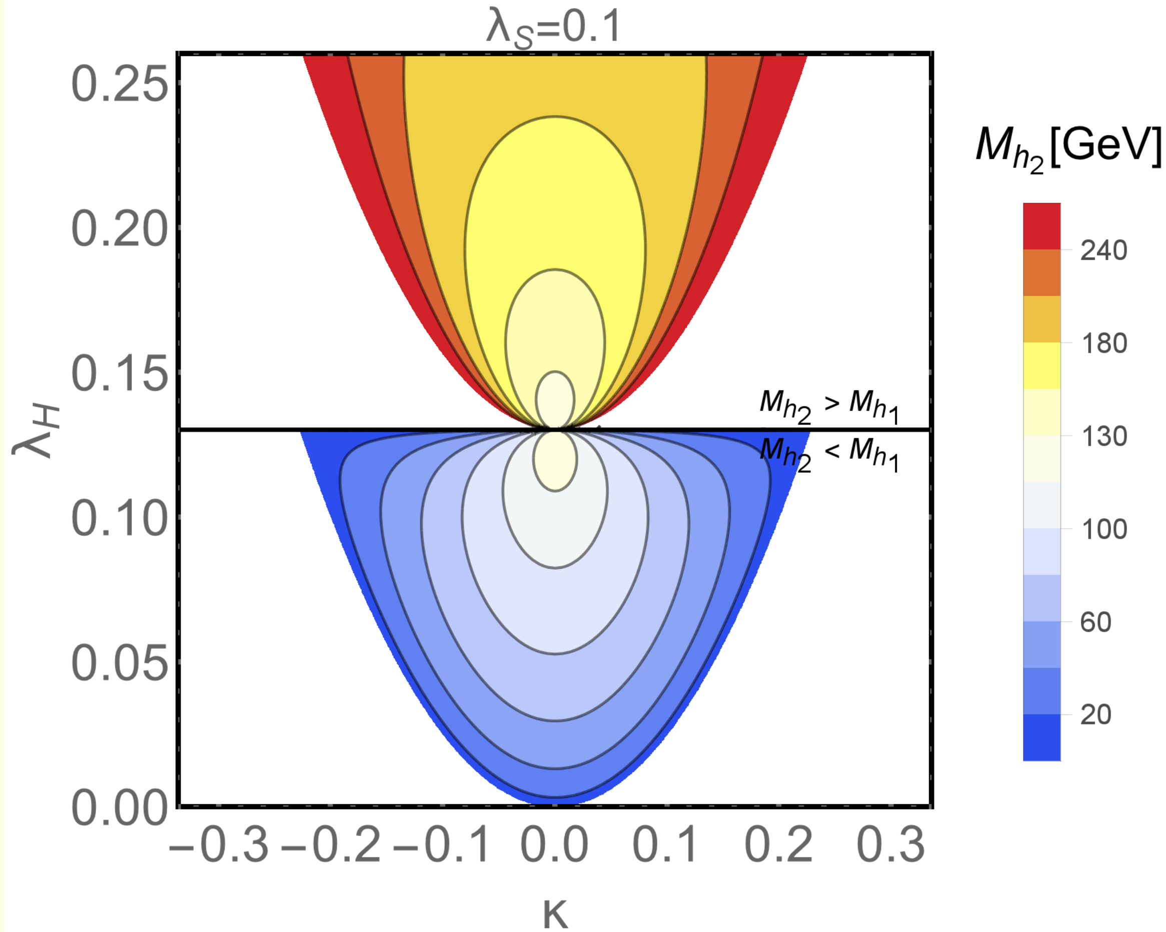

Figure 1: Contour plots for masses of the non-standard (h_2) Higgs particle in the plane (λ_H, κ). In the bottom part of the plot ($\lambda_H < \lambda_{SM} = M^2_{h_1}/(2v^2) = 0.13$) the heavier Higgs is the currently observed one, while in the upper part ($\lambda_H > \lambda_{SM}$) the lighter state is the observed one. White regions in the upper and lower parts are disallowed by the positivity conditions for v_x^2 and $M^2_{h_2}$, respectively.

- Positivity of v_x^2 implies for $\lambda_H > \lambda_{SM}$ that $\lambda_H > \frac{\kappa^2}{4\lambda_S} + \lambda_{SM}$
- Positivity of $M^2_{h_2}$ implies for $\lambda_H < \lambda_{SM}$ that $\lambda_H > \frac{\kappa^2}{4\lambda_S}$

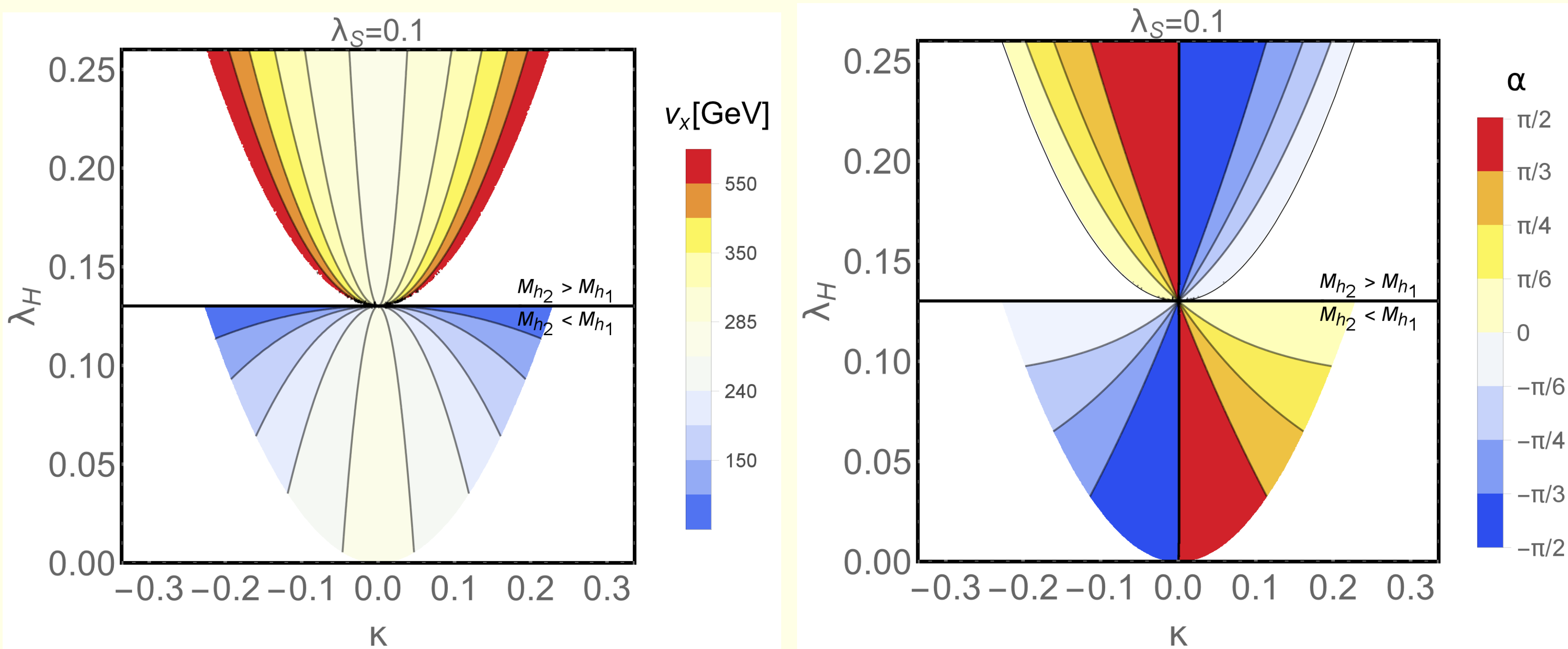

Figure 2: Contour plots for the vacuum expectation value of the extra scalar $v_x \equiv \sqrt{2}\langle S \rangle$ (left panel) and of the mixing angle α (right panel) in the plane (λ_H, κ).

Vacuum stability

$$V = -\mu_H^2|H|^2 + \lambda_H|H|^4 - \mu_S^2|S|^2 + \lambda_S|S|^4 + \kappa|S|^2|H|^2$$

2-loop running of parameters adopted

$$\lambda_H(Q) > 0, \quad \lambda_S(Q) > 0, \quad \kappa(Q) + 2\sqrt{\lambda_H(Q)\lambda_S(Q)} > 0$$

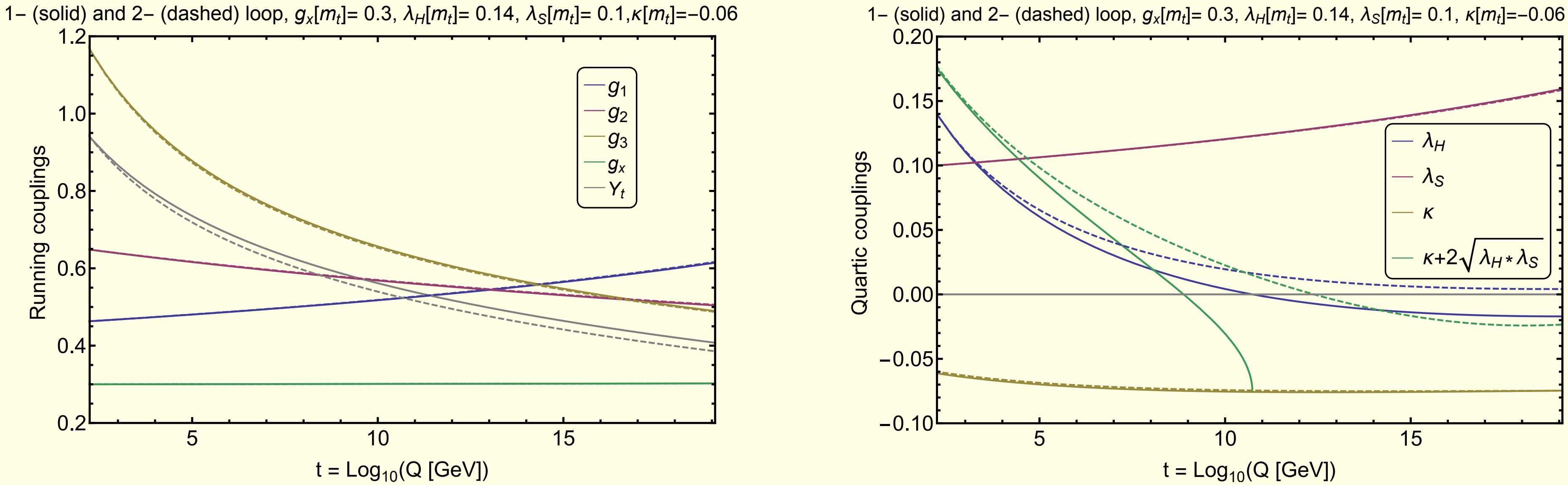

Figure 3: Running of various parameters at 1- and 2-loop, in solid and dashed lines respectively. For this choice of parameters $\lambda_H(Q) > 0$ at 2-loop (right panel blue) but not at 1-loop. $\lambda_S(Q)$ is always positive (right panel red), running of $\kappa(Q)$ is very limited, however the third positivity condition $\kappa(Q) + 2\sqrt{\lambda_H(Q)\lambda_S(Q)} > 0$ is violated at higher scales even at 2-loops (right panel green).

The mass of the Higgs boson is known experimentally therefore within *the SM* the initial condition for running of $\lambda_H(Q)$ is fixed

$$\lambda_H(m_t) = M_{h_1}^2/(2v^2) = \lambda_{SM} = 0.13$$

For VDM this is not necessarily the case:

$$M_{h_1}^2 = \lambda_H v^2 + \lambda_S v_x^2 \pm \sqrt{\lambda_S^2 v_x^4 - 2\lambda_H \lambda_S v^2 v_x^2 + \lambda_H^2 v^4 + \kappa^2 v^2 v_x^4}.$$

VDM:

- Larger initial values of λ_H such that $\lambda_H(m_t) > \lambda_{SM}$ are allowed delaying the instability (by shifting up the scale at which $\lambda_H(Q) < 0$).

- Even if the initial λ_H is smaller than its SM value, $\lambda_H(m_t) < \lambda_{SM}$, still there is a chance to lift the instability scale if appropriate initial value of the portal coupling $\kappa(m_t)$ is chosen.

$$\beta_{\lambda_H}^{(1)} = \beta_{\lambda_H}^{SM\ (1)} + \kappa^2$$

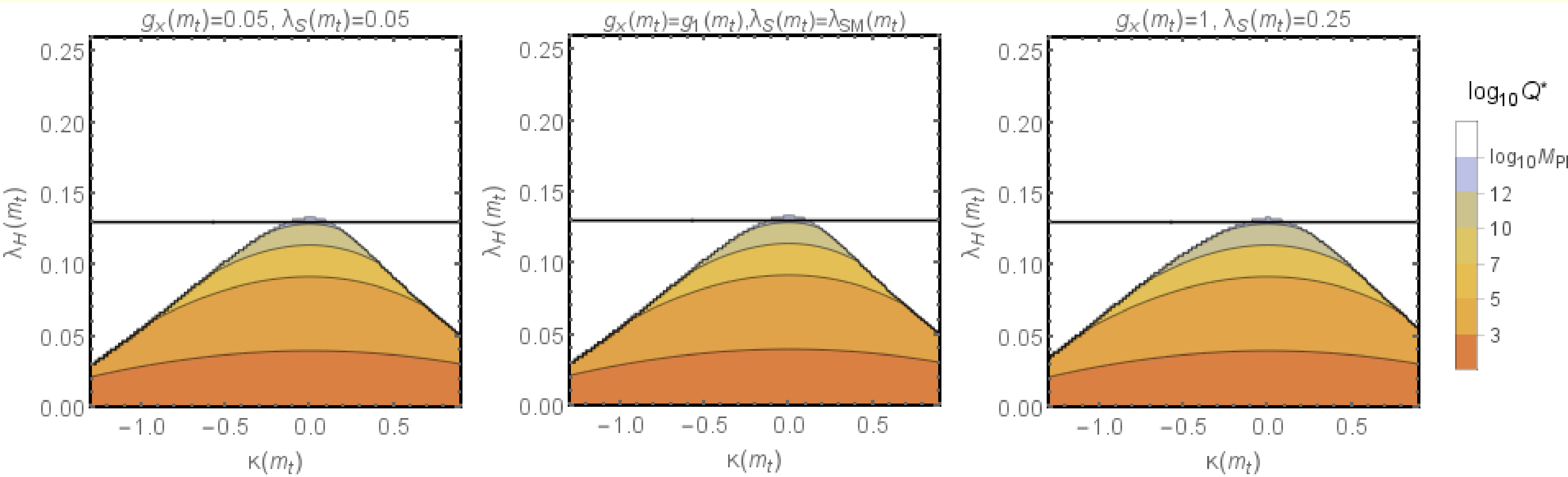

Figure 4: The stability frontier for the H direction: these plots identify the renormalisation scale $t^* = Log_{10}(Q^*)$ at which $\lambda_H(Q^*) = 0$ and the vacuum becomes unstable, as a function of $(\lambda(m_t), \kappa(m_t))$. The horizontal solid black line corresponds to $\lambda_H(m_t) = \lambda_{SM} \simeq 0.13$.

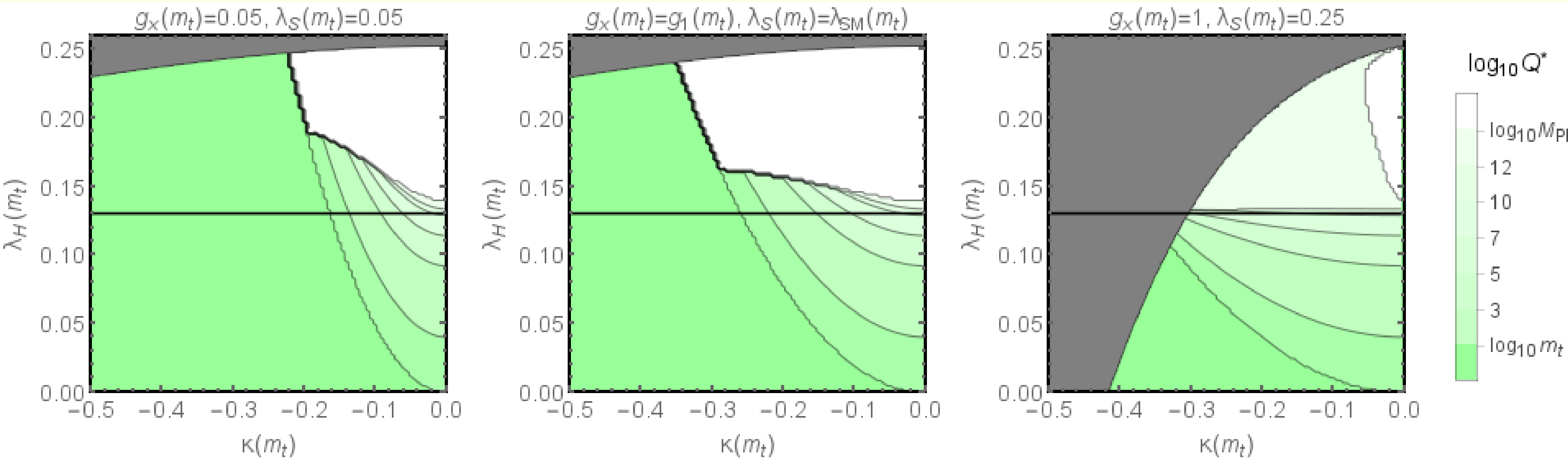

Figure 5: The "in between" stability frontier : these plots identify the scale $t^* = Log_{10}(Q^*)$ at which the positivity condition $\kappa(Q) + 2\sqrt{\lambda_H(Q)\lambda_S(Q)} > 0$ fails and the vacuum becomes unstable, as a function of $(\lambda(m_t), \kappa(m_t))$ for fixed choices of $(g_x(m_t), \lambda_S(m_t))$ specified above each panel. The horizontal solid black line corresponds to $\lambda_H(m_t) = \lambda_{SM} \simeq 0.13$. The gray area is excluded by the requirement that there is no Landau poles up to the Planck mass.

Landau poles

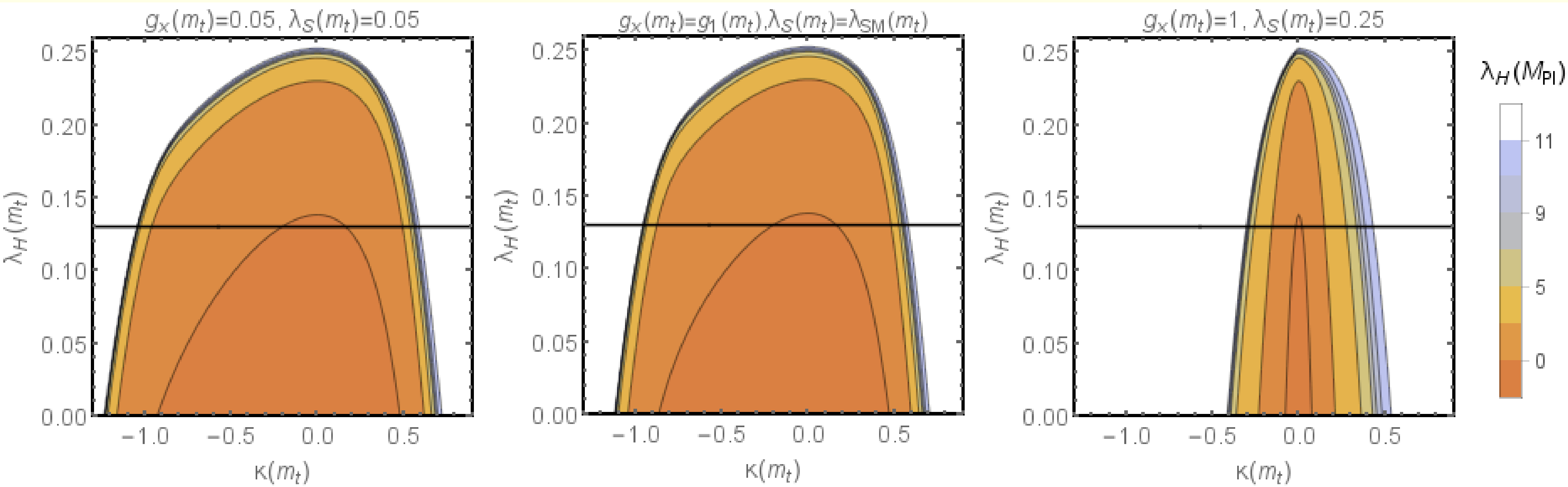

Figure 6: Contour plots of $\lambda_H(M_{Pl})$ in the plane of $(\lambda(m_t), \kappa(m_t))$ for fixed $g_x(m_t)$ and $\lambda_S(m_t)$ specified above each panel. The horizontal solid black line corresponds to $\lambda_H(m_t) = \lambda_{SM} \simeq 0.13$. The plots allow one to identify regions (white) in which the $\lambda_H(Q)$ Landau pole is below the Planck scale.

Experimental constraints

- no invisible h_1 decays: $h_1 \to Z'Z'$, $h_1 \to h_2 h_2$,
- LEP constraints for $e^+e^- \to Z h_2$ satisfied,
- LHC constraints on

$$\kappa_V \equiv \frac{g_{h_1 VV}}{g^{SM}_{h_1 VV}} \ \text{with} \ 0.85 < \kappa_V < 1$$

- limits from electroweak precision data (S,T) satisfied at 95% CL

$$S = \frac{16\pi \cos^2\theta_W}{g^2} \delta\Pi'_{ZZ}(0), \qquad T = \frac{4\pi}{e^2}\left(\frac{\delta\Pi_{WW}(0)}{M_W^2} - \frac{\delta\Pi_{ZZ}(0)}{M_Z^2}\right),$$

- DM abundance ($\Omega_{DM} h^2$) remains within the 5σ limit (micrOMEGAs and explicite calculation)

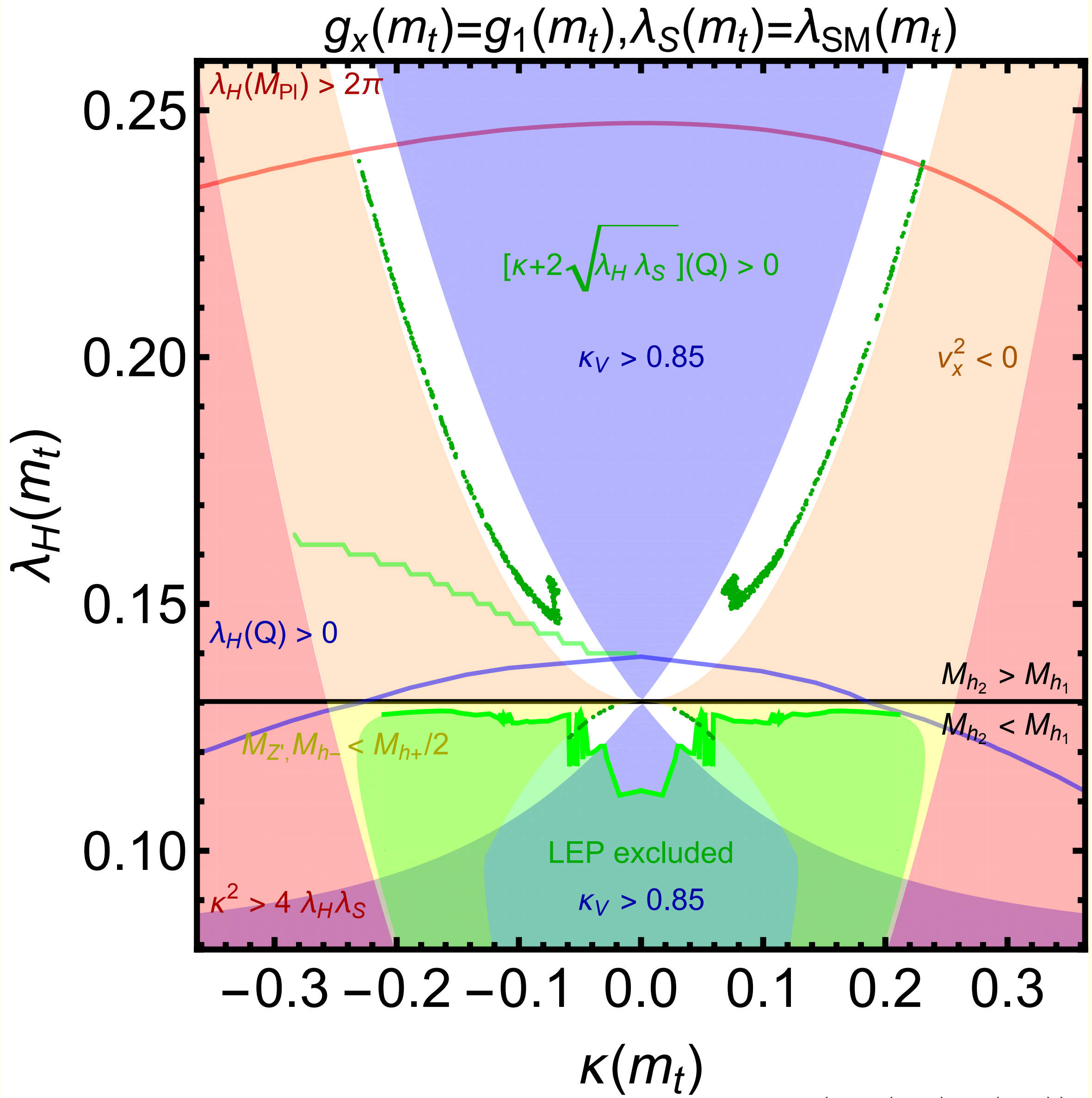

Figure 7: Combined plots of allowed and disallowed parameter space in the plane $(\lambda_H(m_t), \kappa(m_t))$ for $g_x(m_t) = g_1(m_t)$ and $\lambda_S(m_t) = \lambda_{SM}(m_t) = 0.13$. The thin red line denotes the frontier above which a Landau pole appears below $\lambda_H(M_{Pl})$. The thin blue line denotes the absolute stability frontier. Below the thin green line the positivity condition fails at some renormalisation scale (its wavy shape is a numerical artifact). The green area denotes LEP exclusions on Higgs-like scalars. In the outer red area positivity fails at the low scale, while in the orange area no physical solution of the vev v_x exists. The blue area denotes an excess of the h_1 Higgs couplings to vector bosons (κ_V). The remaining allowed region is in white. The green points are those for which also $\Omega_{DM}h^2$ constraint is fulfilled.

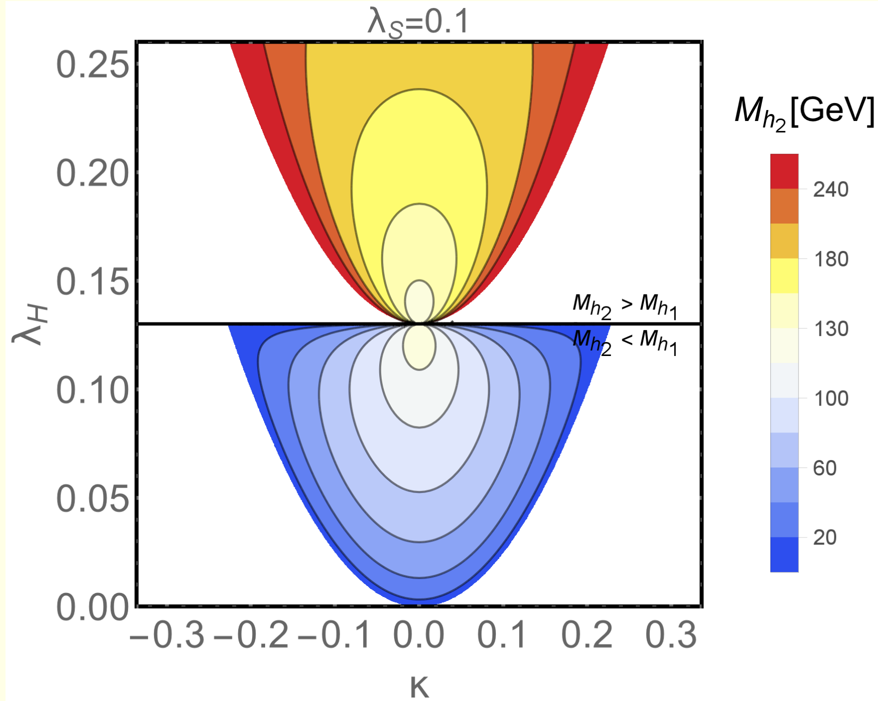
λ_S=0.1
M_{h_2}[GeV]
240
180
130
100
60
20
$M_{h_2} > M_{h_1}$
$M_{h_2} < M_{h_1}$
λ_H
κ

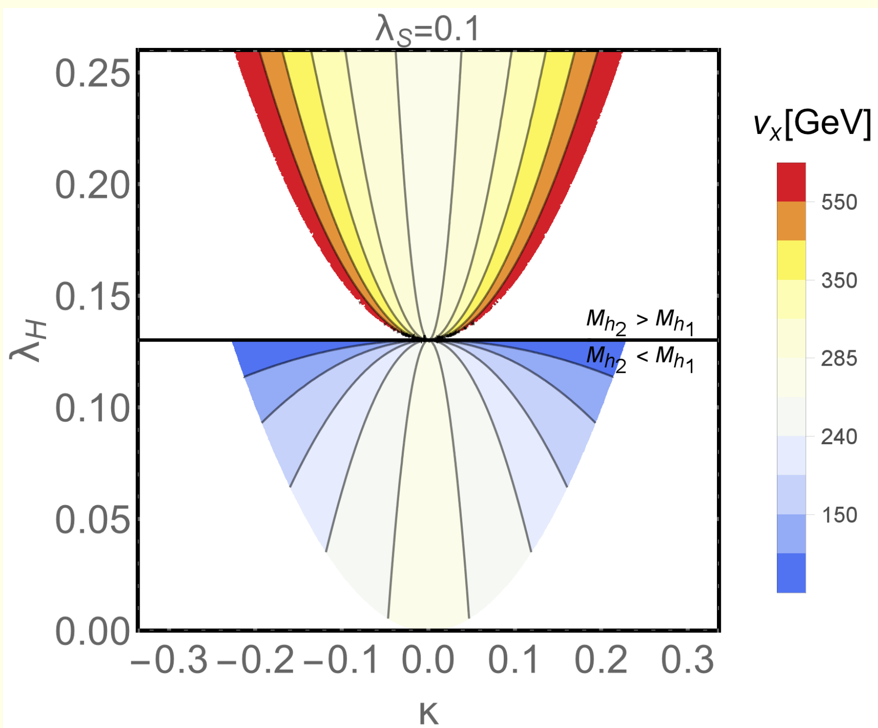
λ_S=0.1
v_x[GeV]
550
350
285
240
150
$M_{h_2} > M_{h_1}$
$M_{h_2} < M_{h_1}$
λ_H
κ

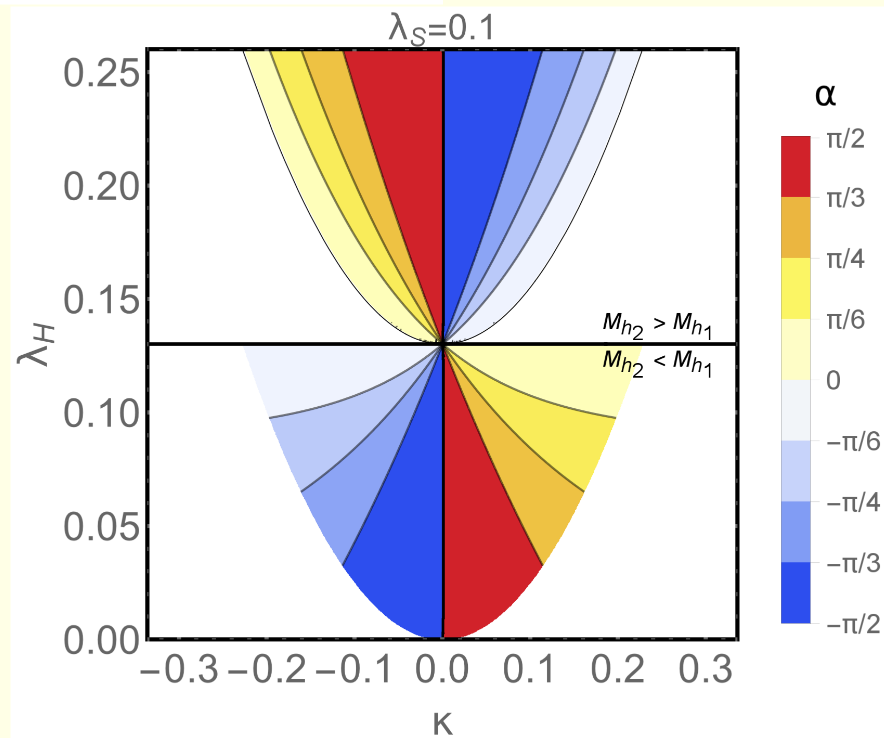
λ_S=0.1
α
π/2
π/3
π/4
π/6
0
−π/6
−π/4
−π/3
−π/2
$M_{h_2} > M_{h_1}$
$M_{h_2} < M_{h_1}$
λ_H
κ

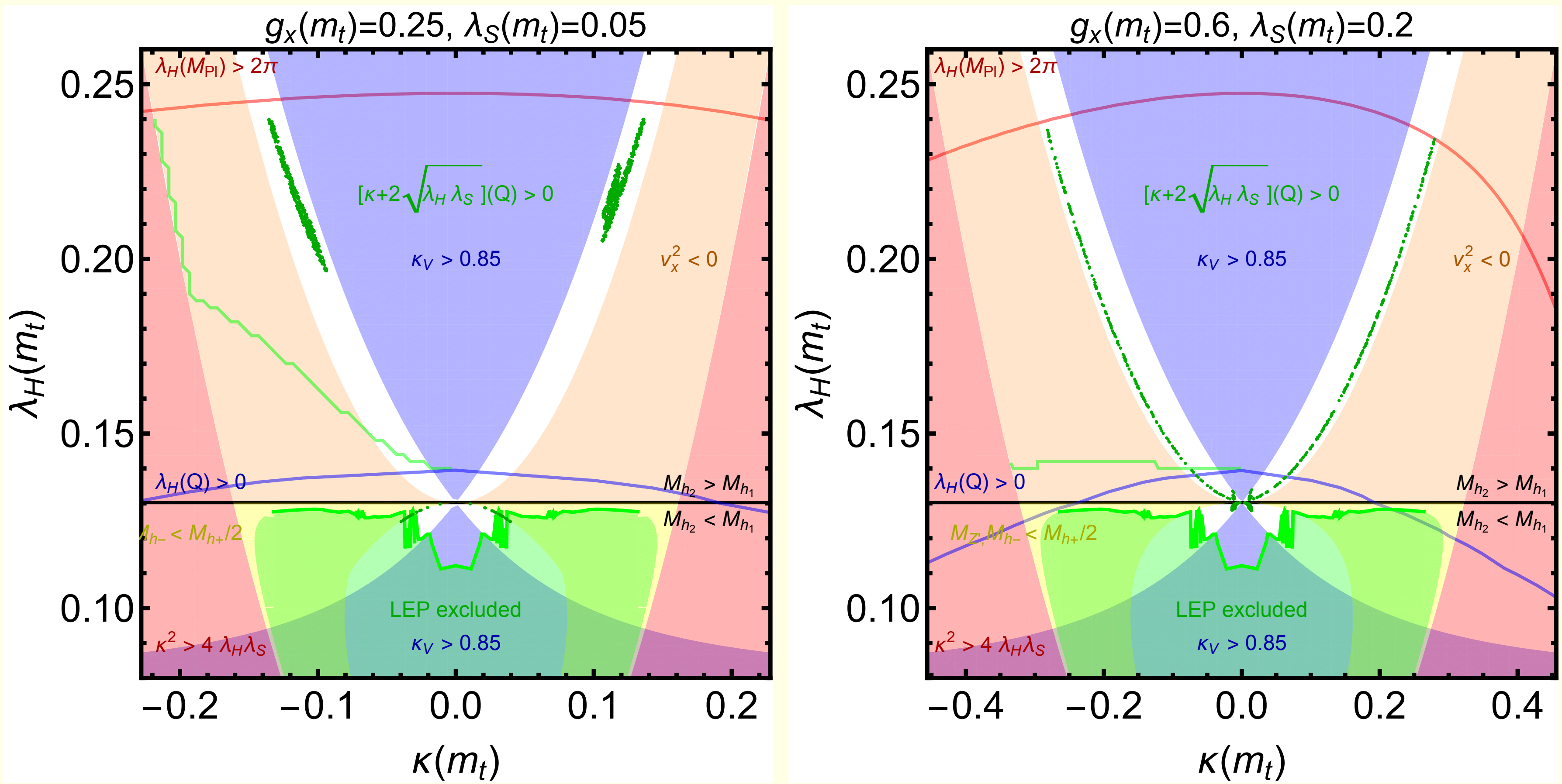
$g_x(m_t)$=0.25, $\lambda_S(m_t)$=0.05
$\lambda_H(M_{Pl}) > 2\pi$
$[\kappa+2\sqrt{\lambda_H \lambda_S}](Q) > 0$
$\kappa_V > 0.85$
$v_x^2 < 0$
$\lambda_H(Q) > 0$
$M_{h_2} > M_{h_1}$
$M_{h_2} < M_{h_1}$
$M_{h-} < M_{h+}/2$
LEP excluded
$\kappa_V > 0.85$
$\kappa^2 > 4\,\lambda_H \lambda_S$
$\lambda_H(m_t)$
$\kappa(m_t)$
$g_x(m_t)$=0.6, $\lambda_S(m_t)$=0.2
$\lambda_H(M_{Pl}) > 2\pi$
$[\kappa+2\sqrt{\lambda_H \lambda_S}](Q) > 0$
$\kappa_V > 0.85$
$v_x^2 < 0$
$\lambda_H(Q) > 0$
$M_{h_2} > M_{h_1}$
$M_{h_2} < M_{h_1}$
$M_{Z'}, M_{h-} < M_{h+}/2$
LEP excluded
$\kappa_V > 0.85$
$\kappa^2 > 4\,\lambda_H \lambda_S$
$\lambda_H(m_t)$
$\kappa(m_t)$

Direct detection of dark matter

$$\sigma_{Z'N} = \frac{\mu^2}{4\pi} g_x^2 g_{hNN}^2 \sin^2 2\alpha \left(\frac{1}{M_{h_1}^2} - \frac{1}{M_{h_2}^2} \right)^2$$

- scan range: $0.1 < g_x < 1, 0 < \lambda_H < 0.25$ and $-0.5 < \kappa < 0.5$
- $\lambda_H < \lambda_{SM}$ (light dark matter): 60 GeV $\lesssim M_{Z'} \lesssim$ 120 GeV,
- $\lambda_H > \lambda_{SM}$ (heavy dark matter): 63 GeV $\lesssim M_{Z'} \lesssim$ 1000 GeV.

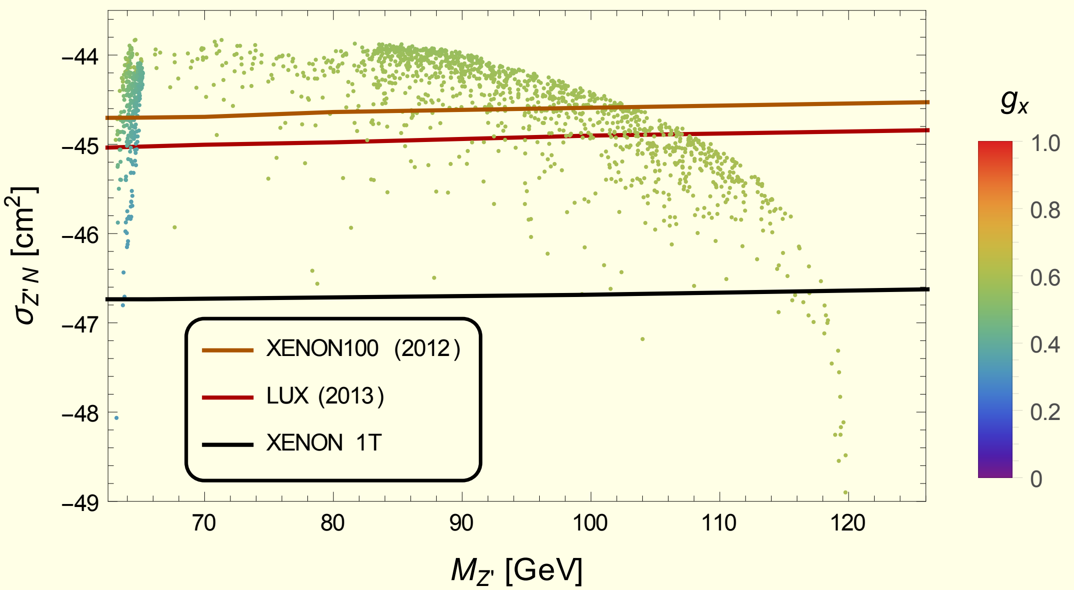

Figure 8: The figure shows the DM-nucleon cross section, $\sigma_{Z'N}$, as a function of the DM mass $M_{Z'}$ for points which satisfy all other constraints for $\lambda_H < \lambda_{SM}$. The singlet quartic coupling is fixed at $\lambda_S = 0.2$. Colouring corresponds to the strength of the gauge coupling g_x. The nearly horizontal lines are the experimental limits for $\sigma_{Z'N}$ from XENON100, LUX (2103) and anticipated results for XENON 1T.

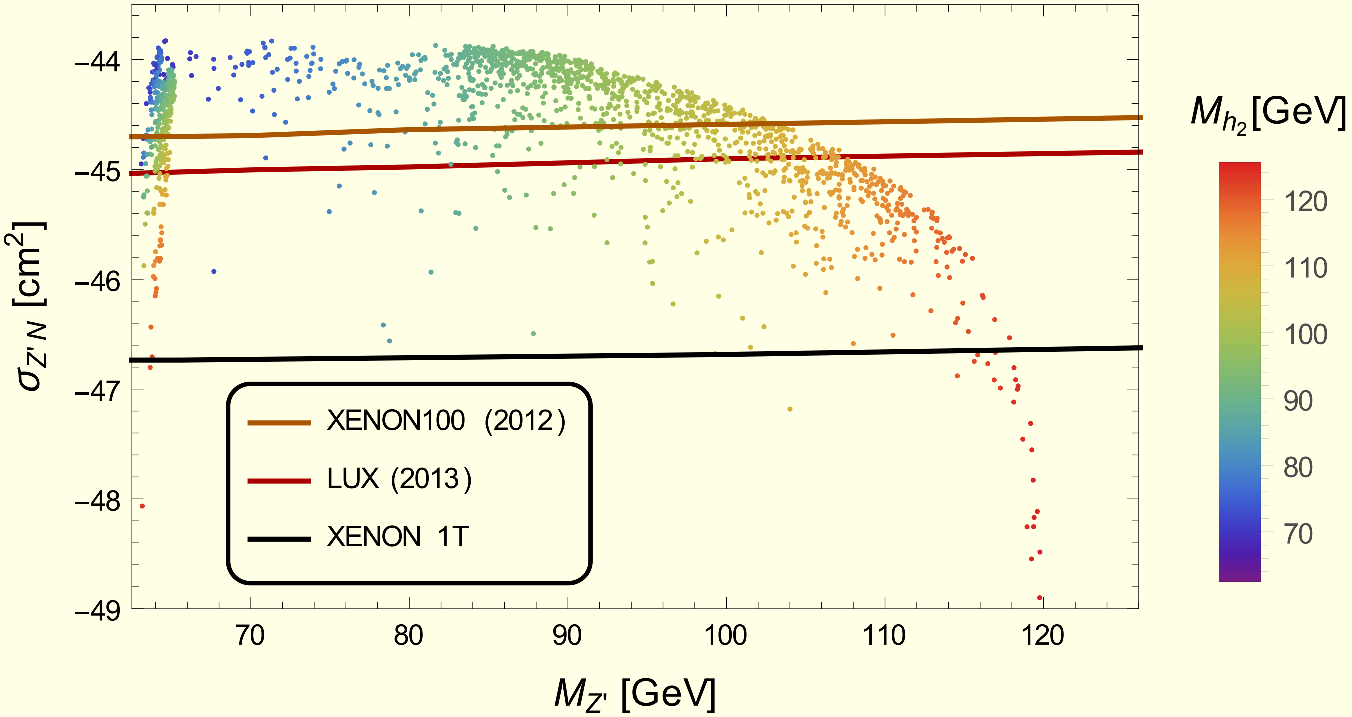

M_{h_2}[GeV]
120
110
100
90
80
70
XENON100 (2012)
LUX (2013)
XENON 1T
$\sigma_{Z'N}$ [cm^2]
−44
−45
−46
−47
−48
−49
70
80
90
100
110
120
$M_{Z'}$ [GeV]

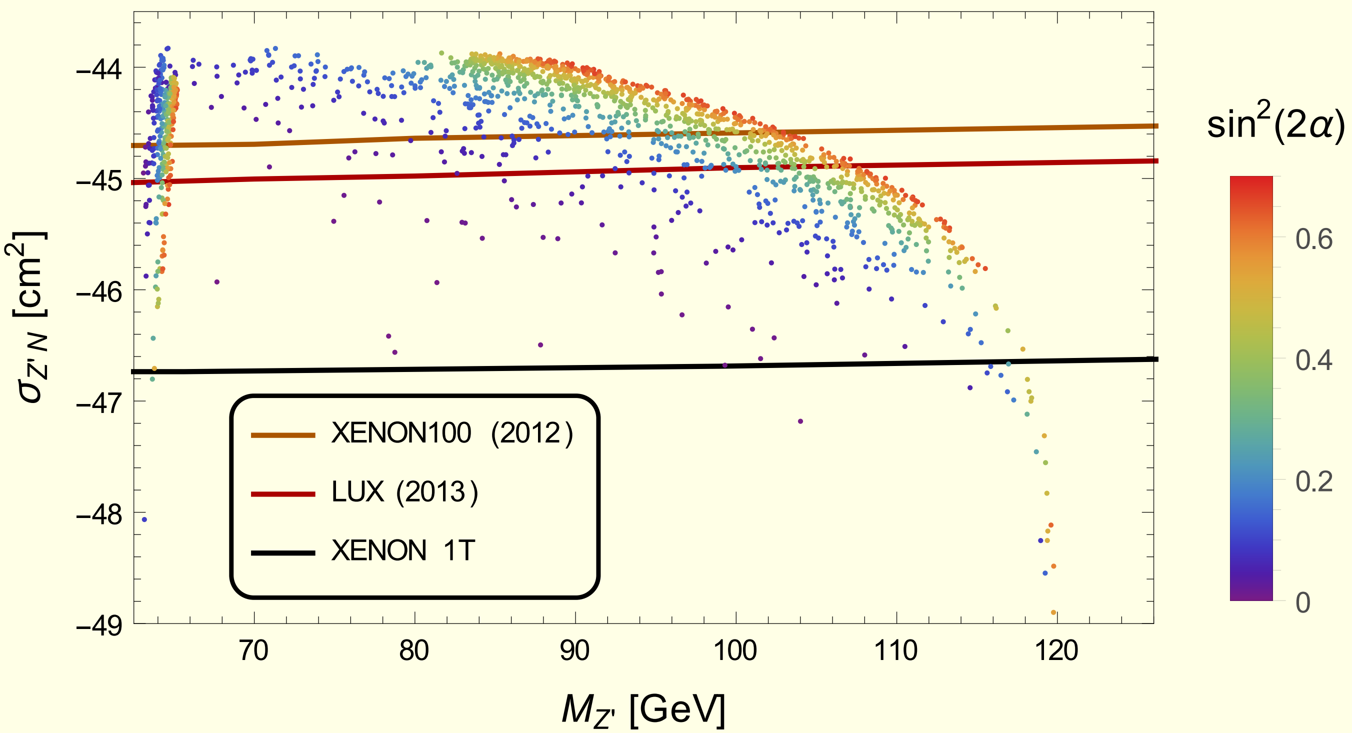

$\sin^2(2\alpha)$
0.6
0.4
0.2
0
XENON100 (2012)
LUX (2013)
XENON 1T
$\sigma_{Z'N}$ [cm^2]
−44
−45
−46
−47
−48
−49
70
80
90
100
110
120
$M_{Z'}$ [GeV]

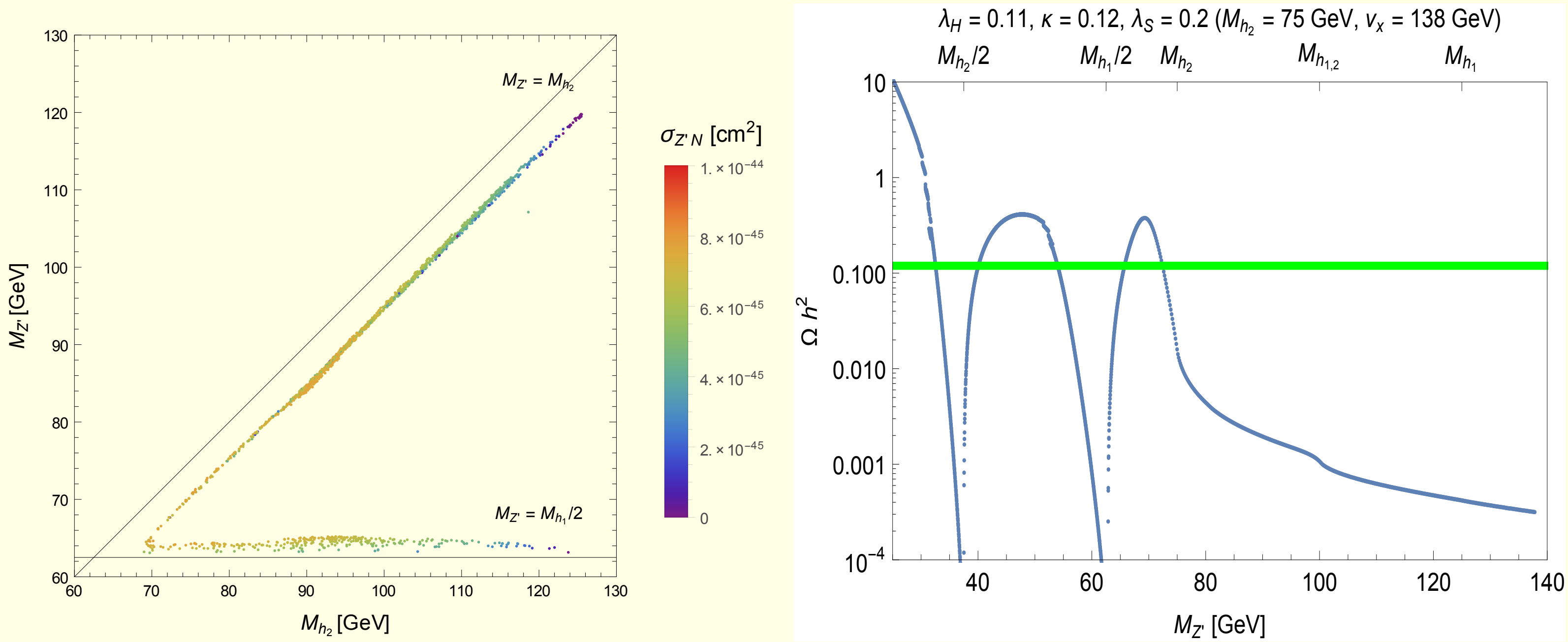

Figure 9: The left panel illustrates correlation between between M_{h_2} and $M_{Z'}$, while the right one shows predictions for $\Omega_{DM}h^2$ as a function of $M_{Z'}$. The colouring corresponds to the cross section $\sigma_{Z'N}$. Above the right box resonances and channels which open as $M_{Z'}$ increases are shown. Coordinates in the parameter space $(\lambda_H, \kappa, \lambda_S)$ and corresponding M_{h_2} and v_x are shown above the right panel.

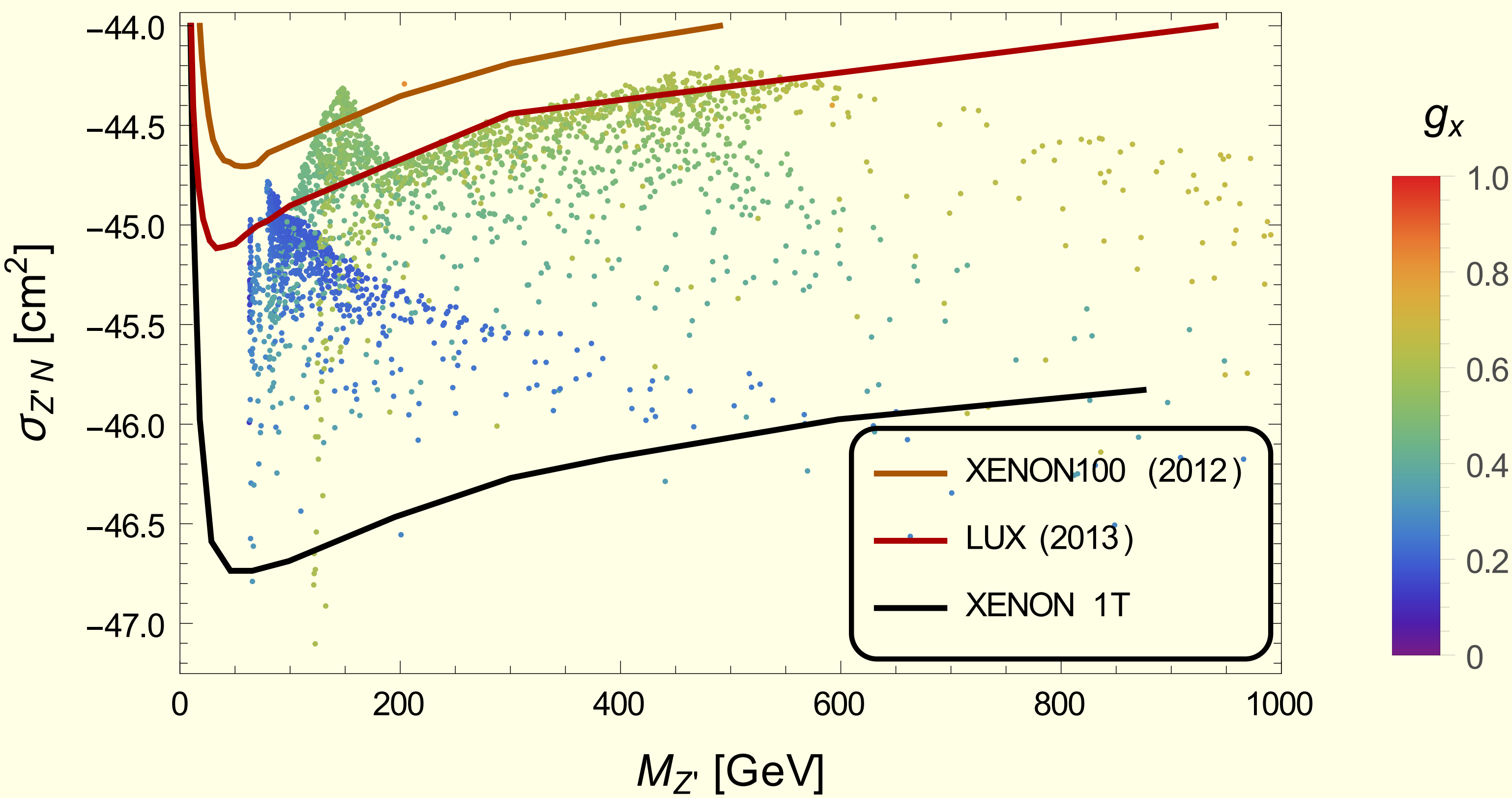

Figure 10: The figure shows the DM-nucleon cross section, $\sigma_{Z'N}$, as a function of the DM mass $M_{Z'}$ for points which satisfy all other constraints for $\lambda_H > \lambda_{SM}$. The singlet quartic coupling is fixed at $\lambda_S = 0.2$. Colouring corresponds to the strength of the gauge coupling g_x. The solid lines are the experimental limits for $\sigma_{Z'N}$ from XENON100, LUX (2103) and anticipated results for XENON 1T.

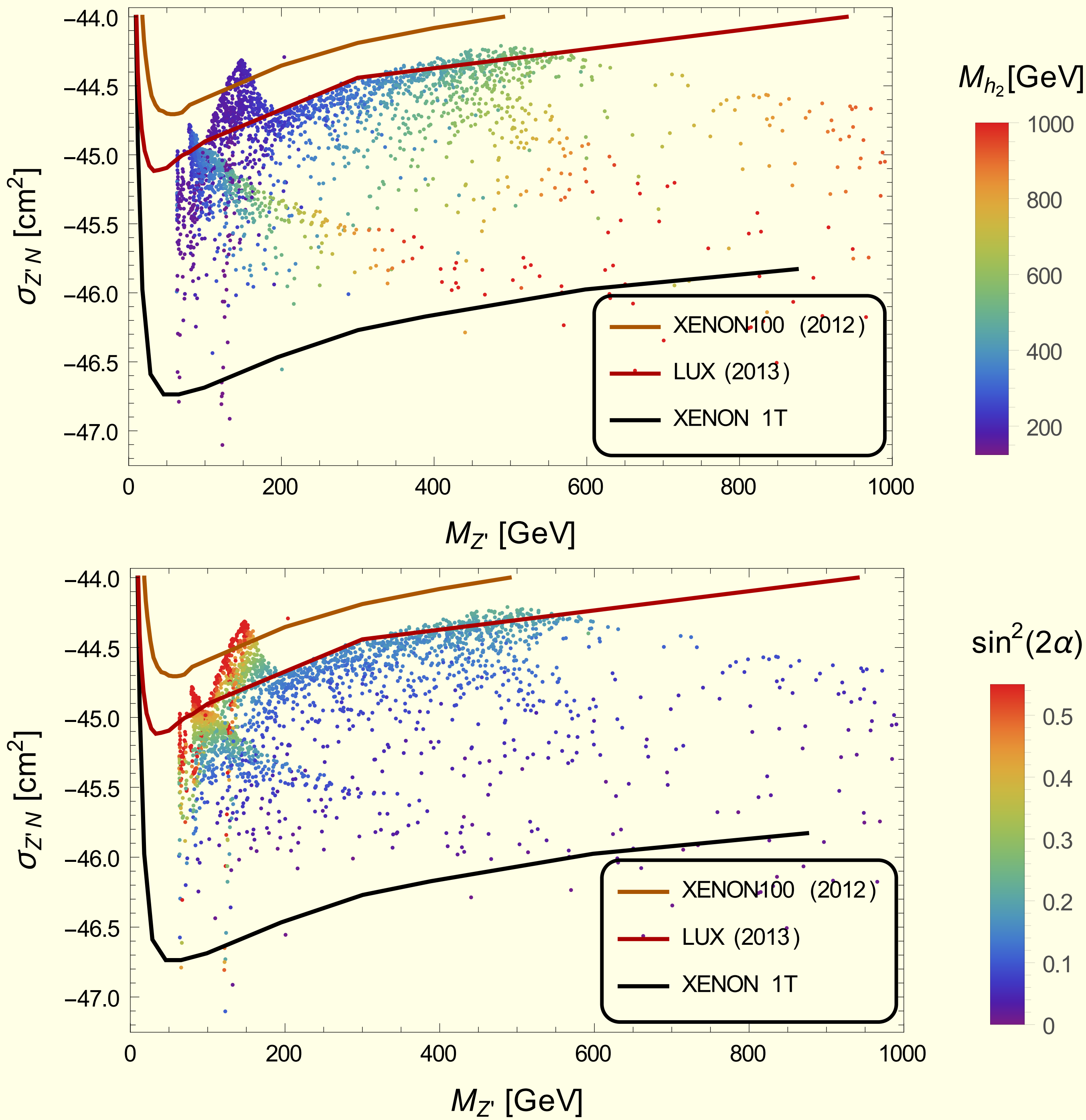
M_{h_2}[GeV]
1000
800
600
400
200
$\sigma_{Z'N}$ [cm^2]
−44.0
−44.5
−45.0
−45.5
−46.0
−46.5
−47.0
0
200
400
600
800
1000
$M_{Z'}$ [GeV]
XENON100 (2012)
LUX (2013)
XENON 1T
$\sin^2(2\alpha)$
0.5
0.4
0.3
0.2
0.1
0

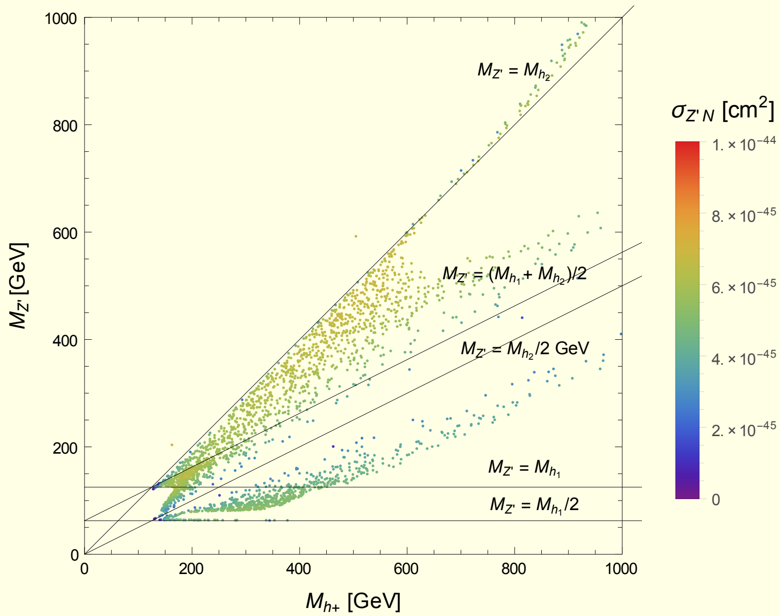

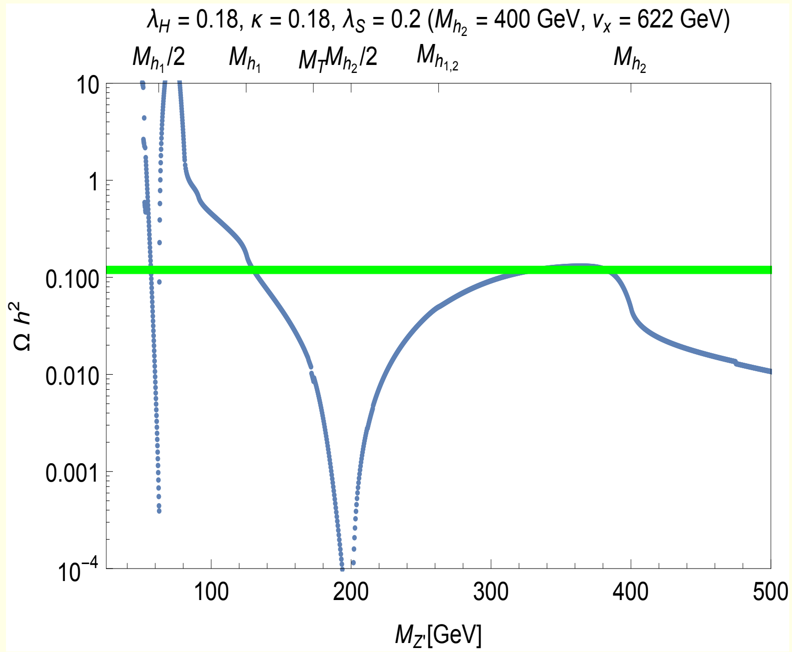

Figure 11: The left panel illustrates correlation between between M_{h_2} and $M_{Z'}$, while the right one shows predictions for $\Omega_{DM}h^2$ as a function of $M_{Z'}$. The colouring corresponds the the cross section $\sigma_{Z'N}$. Above the right box resonances and channels which open as $M_{Z'}$ increases are shown. Coordinates in the parameter space $(\lambda_H, \kappa, \lambda_S)$ and corresponding M_{h_2} and v_x are shown above the right panel.

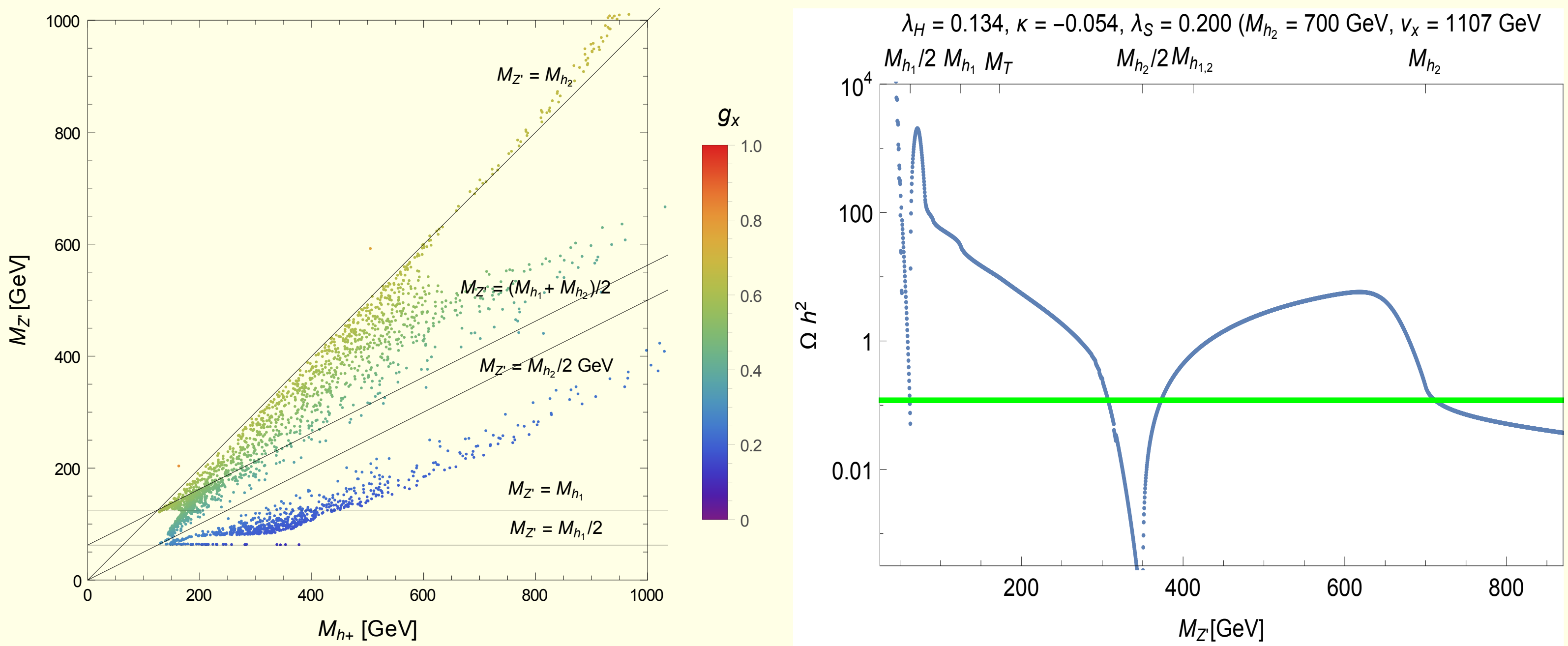

Figure 12: The left panel illustrates correlation between between M_{h_2} and $M_{Z'}$, while the right one shows predictions for $\Omega_{DM}h^2$ as a function of $M_{Z'}$. The colouring corresponds to the cross section g_x. Above the right box resonances and channels which open as $M_{Z'}$ increases are shown. Coordinates in the parameter space $(\lambda_H, \kappa, \lambda_S)$ and corresponding M_{h_2} and v_x are shown above the right panel.

Summary

- VDM model has been presented: Z' (DM), h_2 (extra Higgs)
- Vacuum stability was addressed: absolute stability
- Cosmological consequences were discussed, VDM easily consistent with $\Omega_{DM}h^2$ and $\sigma_{Z'N}$